Draft version September 23, 2016
Preprint typeset using LaTeX style AASTeX6 v. 1.0

CLOUDS ON A WATER RUNAWAY GREENHOUSE

Matej Malik[1] and Colin Goldblatt[2]

[1]University of Bern, Center for Space and Habitability, Sidlerstrasse 5, CH-3012, Bern, Switzerland. Email: matej.malik@csh.unibe.ch
[2]School of Earth and Ocean Sciences, University of Victoria, PO Box 3065, Victoria, British Columbia, V8W 3V6, Canada

ABSTRACT

We explore the effect of clouds on earth-centric pure water atmospheres by using a 1D column grid and the radiative-convective transfer model SMART. Specifically, we are interested whether the clouds enhance or hinder the establishment of the runaway greenhouse mechanism over a wide range of temperatures motivated by the findings of Goldblatt et al. (2013) for a clear-sky atmosphere. We determine the cloud location and density by simple first principle considerations and manually tune the cloud optical depth to explore a wide parameter space. In our nominal case, the clouds are located at 10^{-3}–10^{-2} bar and their optical depth is 1.7 or 17, respectively. We assume a log-normal condensate size distribution centered at 10 μm. We find for these settings a negative cloud forcing. The increase of the planetary albedo due to the clouds is larger than their contribution to the greenhouse effect. Moreover, sufficiently thick clouds with $\tau_{\rm cloud} \gtrsim 0.6$ prevent the runaway mechanism completely by installing a stable atmospheric equilibrium state. The required cloud thickness increases for smaller cloud coverage fractions, but no stable solution is found for a fraction of less than 0.02. Using a test case with a surface temperature of 645 K, we probe the cloud forcing in detail in order to find the physical reasons for the negative cloud forcing. Since the clouds are located high above the optical photosphere but roughly coincide with the thermal photosphere their impact on the shortwave radiation is stronger, thus explaining the net cooling. Changing the cloud particle size distribution from a log-normal to a bimodal gamma distribution, as would be the case for two distinct condensate populations like liquid droplets and ices, somewhat weakens the negative cloud forcing. Still, in our set-up the latter effect is only significant for clouds with $\tau_{\rm cloud} = 17$ and not for clouds with $\tau_{\rm cloud} = 1.7$ or thinner.

1. INTRODUCTION

The runaway greenhouse is an atmospheric unstable state where the atmosphere is unable to emit as much radiation as it absorbs, leading to a runaway global warming. There are two classic limits to the thermal emission of a planet. The Komabayashi-Ingersoll limit describes the maximum outgoing flux due to stratospheric and tropospheric coupling in radiative equilibrium (Komabayashi 1967; Ingersoll 1969). An increased tropospheric emission corresponds to an increased stratospheric emission only until the tropopause temperature reaches a limit, from which point on this relation reverses. Above this temperature sufficient heat release is prevented and thus runaway warming establishes. Usually this stratospheric limit is not reached, because of the lower Simpson-Nakajima limit (Simpson 1927; Nakajima et al. 1992). Let us assume we have a sufficiently large surface liquid water reservoir. Upon heating the surface, liquid water evaporates increasing the vapour mixing ratio in the atmosphere. As evaporation continues the tropospheric temperature asymptotically approaches the saturation vapour-pressure curve. Since the optical depth is directly proportional to the pressure the atmospheric photosphere ($\tau_{\rm therm} \approx 1$) will be at the same temperature, limiting the emission independently of the surface temperature. That surface heating from external sources is possible while the thermal outgoing emission is constrained is a consequence of the strong greenhouse nature of water. It is optically thicker in the thermal (longwave) than in the optical (shortwave), thus the incoming radiation is deposited in deeper layers than the region of main emission.[1]

A compact summary of the atmospheric radiation limits, their role for the runaway greenhouse effect and the possible implications for the current Earth system are discussed in Goldblatt & Watson (2012).

[1] The region of main absorption and emission is characterized by an optical depth around unity and called the photosphere. It is usually wave-length dependent.

1.1. *Scientific Goal*

We use the Goldblatt et al. (2013) as basis for our study. They explored the runaway greenhouse for Earth with a clear-sky atmosphere. They assumed a pure water atmosphere, which for higher temperatures is a good approximation, since through evaporation the water mixing ratio becomes close to unity. They found a limit of 286 W m^{-2} for the net incoming shortwave flux and the limit of 282 W m^{-2} for the net outgoing longwave flux (the Simpson-Nakajima limit) for a wide range of surface temperatures ($\sim$ 500 - 1600 K). Due to this 4 W m^{-4} surplus of incoming radiation, the planet is caught in a runaway warming. Only at higher than 1600 K, the planet starts to emit sufficiently through the near-infrared water band windows to reach a stable equilibrium state.

We use their pure water set-up and numerical method and include a simple cloud model. We are interested in the radiative effect of clouds on the atmosphere and want to determine whether clouds enhance or hinder the establishment of the runaway greenhouse mechanism.

1.2. *Layout*

In Section 2, we elucidate the properties of the radiative transfer scheme and of the utilized clouds. For the latter, we do not have the resources to incorporate a micro-physics. Hence, we focus on a cloud parameterization that is physically motivated yet flexible enough to allow for a wide exploration of the relevant parameter space. To reach this aim, we need to answer two questions:

- What is a plausible location and extent of clouds in terms of altitude or atmospheric pressure? In short: *"Where are the clouds?"*
- What is the impact of the clouds on the radiative energy budget of the atmosphere? As this is given by the integrated optical depth of the cloud aerosols, we are interested in their density and size distribution. In short: *"How thick are the clouds?"*

We investigate these motives in Sections 2.3 - 2.6.

In Section 3, we show our results. Amongst others, we discuss the effect of clouds on the runaway greenhouse over a wide temperature regime (Sec. 3.1) and analyze the cloud forcing in detail (Sec. 3.2). Finally, we compare our findings to previous work and conclude in Section 4.

2. METHOD

2.1. *Radiative Transfer Model*

In order to pinpoint the effect of clouds on an atmosphere we choose the model set-up as simple as possible while still incorporating the whole cloud physics. For this we restrain our study to a one-dimensional azimuthally averaged grid. The radiative transfer is calculated with the Spectral Mapping and Atmospheric Radiative Transfer (SMART) code (Meadows & Crisp 1996), based on the DISORT model (Stamnes et al. 1988), which solves the radiative transfer equation using the discrete ordinates method for multiple discrete ray scattering directions ("*streams*"). The up- and downward radiative fluxes are computed through inversion of the matrix containing the angular information. For a given atmospheric structure, with pre-tabulated scattering cross-sections, absorption coefficients and molecular abundances, the SMART code calculates the spectral (i.e. wavelength-dependent) and integrated fluxes, providing the planetary spectral energy distribution and the atmospheric heating rates, respectively. In our set-up we choose 8 streams for the scattering and approximate a mean dayside hemispheric geometry with a solar zenith angle of 57°.[2]

2.2. *Atmospheric Properties*

Our model mimics the Earth's atmosphere, modelled by a plane-parallel horizontally layered grid vertically distributed by the logarithm of the pressure P. The top of the computational domain, which we regard as the top of atmosphere (TOA), is at $P = 10^{-5}$ bar and the bottom is given by the surface pressure. The surface gravity is $g = 9.81$ m s^{-2} and assumed constant in the modelled atmosphere, as its vertical extent, $z \lesssim 550$ km, is small compared to the planet's radius $R = 6371$ km. The orbital separation is $a = 1$ AU. The stellar irradiation is given by a solar Kurucz (ATLAS) spectrum and accordingly weighted by the orbital separation. In order to avoid the spectral "noise" of different molecular species we pick a pure water atmosphere with a H_2O mixing ratio of unity throughout the atmosphere and hence an atmospheric mean molecular weight of 18 g mol^{-1}. Rayleigh scattering due to H_2O and H_2O - H_2O collision-induced absorption (CIA) are added to the usual H_2O line absorption. Additionally, a surface liquid water content of one Earth's ocean is assumed, which is needed to trigger the runaway greenhouse.

2.2.1. *Temperature Profile*

In order to explore the runaway greenhouse in a wide temperature regime we assume surface temperatures $T_{\rm surf}$ in the range 280 K $\leq T_{\rm surf} \leq$ 2000 K (see Fig. 1). The corresponding atmospheric temperature profiles follows the moist adiabatic lapse rate, which is the

[2] Due to numerical issues, we choose a slightly different angle than the geometric average of 60°. Such a small deviation has no influence on the findings of this study.

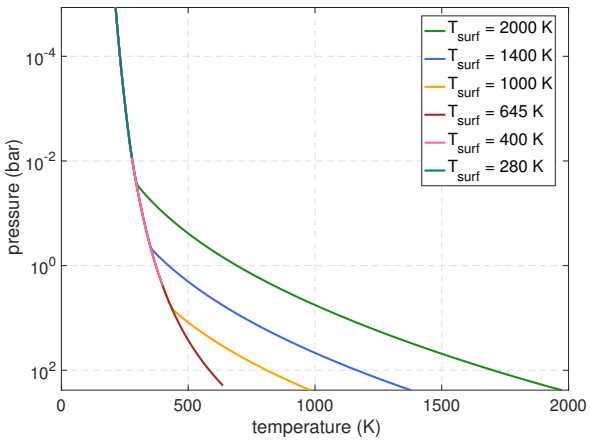

Figure 1. The atmospheric temperature profile for a range of surface temperatures (different colors). Below the critical point of water ($T = 645$ K) the profile follows the water-vapour saturation curve and above the dry adiabat. Through evaporation of liquid surface water the surface pressure increases with surface temperature until $P_{\rm surf} \approx 220$ bar, at which point all liquid water is exhausted.

empirically found structure of the troposphere.[3] In a pure water atmosphere, such a profile coincides with the water-vapour saturation curve. In this set-up the troposphere extends until the TOA so that the stratosphere is not modelled. This simplification is acceptable as the impact of the optically thin atmosphere on radiative transfer above 10^{-5} bar is minor. As the surface temperatures increase, liquid water from the surface evaporates adding to the total atmospheric pressure. Thus, the surface pressure increases with the surface temperature until all the liquid water content is exhausted. The final bottom of atmosphere (BOA) is at $P \approx 220$ bar. Once the surface temperature exceeds the critical point of water, located at T = 645 K, no latent heat due to phase transitions is released or absorbed as water becomes a super-critical fluid. Hence, in this regime the temperature profile follows the dry adiabatic lapse rate.

2.3. *Cloud Location*

Clouds form when atmospheric gas condenses out. Since the phase transition from vapour to liquid is an exothermic process, latent heat is released into the region of the atmosphere where cloud formation occurs. This latent heat release manifests itself in a positive convective flux divergence, analogously as the divergence of the radiative flux leads to atmospheric heating or cooling. In this sense, clouds are a natural by-product of convection and are found where condensation leads to a positive convective flux divergence. Thus, in order to constraint the cloud location in the atmosphere, we search the atmospheric regions marked with a positive convective flux divergence.

We start with a clear-sky situation and assume for a given surface temperature (e.g. $T_{\rm surf} = 645$ K) the corresponding tropospheric temperature profile. Considering only radiation, the atmosphere will not be in equilibrium, because the deposited radiative net flux is positive (see Fig. 2, left panel), leading to a net warming of the atmosphere. However, together with convection, radiative-convective equilibrium can be established if we demand

$$F_{\rm net,rad} + F_{\rm net,conv} = 0, \tag{1}$$

where $F_{\rm rad,net}$ and $F_{\rm conv,net}$ are the net radiative and convective fluxes. In general, we define the net flux as $F_{\rm net} = F_{\downarrow} - F_{\uparrow}$, which physically corresponds to the net power deposited below the probed location. By differentiating eq. (1), one obtains the local net convective flux divergence through

$$\frac{\partial F_{\rm net,conv}}{\partial z} = -\frac{\partial F_{\rm net,rad}}{\partial z}, \tag{2}$$

shown in the right panel of Fig. 2. Following the above argumentation, we expect the cloud condensates to be found in the region of positive convective flux divergence between aprox. $10^{-1.5}$ bar and 10^{-4} bar. Analogously, a negative convective flux divergence would be an indication for evaporation as found in this case in the deeper layers around 1 bar. For our study we neglect evaporating processes and focus only on the condensing parts of the atmosphere.

2.4. *Cloud density*

For the following we consider an imaginary box located in the cloud forming region of the atmosphere (see Fig. 3). The size of the box is small enough so that the atmospheric pressure is assumed constant within the box. Since the latent heat gives the energy released per mass of water, it is possible to connect the convective flux divergence to the condensation rate by

$$\frac{\partial \rho_{\rm cond}}{\partial t} = \frac{\partial F_{\rm net,conv}}{\partial z}\frac{1}{L_{\rm heat}}, \tag{3}$$

where $\partial\rho_{\rm cond}/\partial t$ is the condensate mass density gained in the box per unit time and $L_{\rm heat}$ is the latent heat released per unit mass. The condensates aggregate and grow until being rained out since with increasing particle size gravity eventually exceeds the updraft force. In our toy model we neglect the particle growth processes and focus instead on the macroscopic interplay between condensation and rainout. In equilibrium the condensation rate should be equal to the rainout density loss rate

[3] Physically this means that convection is more efficient than radiation at transferring heat.

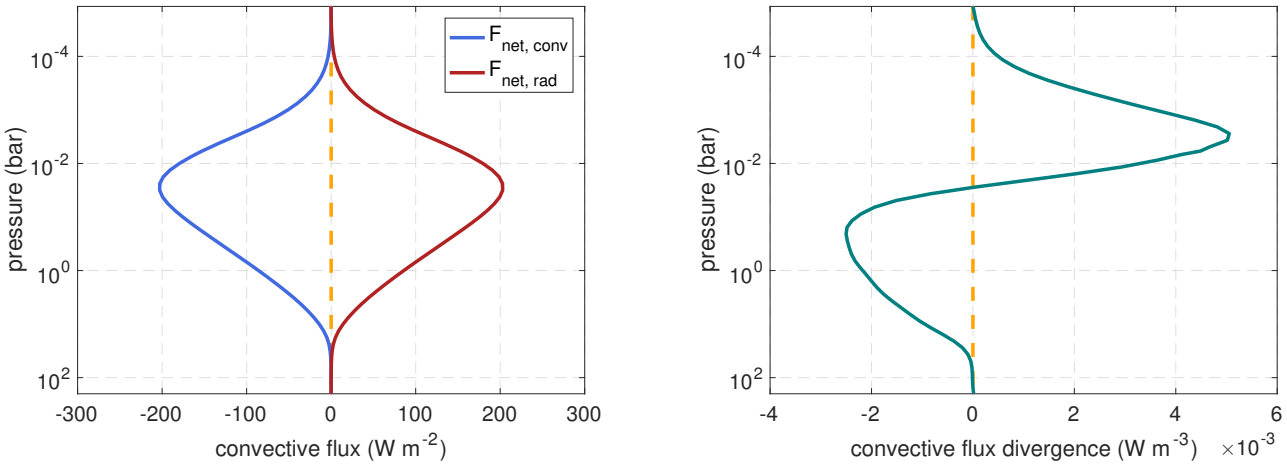

Figure 2. The net convective flux (left panel, blue) required to reach radiative-convective equilibrium in a clear-sky atmosphere with $T_{\rm surf} = 645$ K. Under equilibrium conditions the sum of the net convective and radiative (red) fluxes vanishes. The divergence of the net convective flux (right panel) represents the atmospheric regions of latent heat release and absorption. Since the condensation process releases heat, clouds are expected, where the divergence of the net convective flux is positive. In this case, it is between aprox. $10^{-1.5}$ bar and 10^{-4} bar.

from the box $\partial\rho_{\rm rain}/\partial t$ so that

$$\frac{\partial\rho_{\rm cloud}}{\partial t} = \frac{\partial\rho_{\rm cond}}{\partial t} + \frac{\partial\rho_{\rm rain}}{\partial t} = 0, \tag{4}$$

with the total box cloud density $\rho_{\rm cloud}$ being constant with time. The rainout density loss rate can be approximated by

$$\frac{\partial\rho_{\rm rain}}{\partial t} = \rho_{\rm cloud}\frac{v_{\rm rain}}{\Delta z}, \tag{5}$$

where $v_{\rm rain}$ is the rainout velocity and Δz is the box height. In the macroscopic regime (particle size $\gtrsim 0.1$ mm)[4] the rainout velocity can be estimated by equating the gravity and drag forces, which leads to

$$v_{\rm rain} = \sqrt{\frac{8}{3}\frac{\rho_{\rm w} g R_{\rm univ}}{\bar{m}}}\sqrt{\frac{Tr}{P}}, \tag{6}$$

where $\rho_{\rm w}$ is the water mass density, $R_{\rm univ}$ is the universal gas constant, $\bar{m}$ is the mean atmospheric molar mass and r is the particle size. When combining eq. (3), (4), (5) and (6) we obtain

$$\rho_{\rm cloud} = \frac{\partial F_{\rm net,conv}}{\partial z}\frac{\Delta z}{L_{\rm heat} v_{\rm rain}}, \tag{7}$$

for the total cloud density. It is inversely proportional to the rainout velocity, as would be expected. For a fixed condensation rate the bulk of the cloud is therefore shifted towards higher pressures (lower altitude), since the rainout velocity depends inversely on the pressure (see eq. 6). In our model we set to rainout particle size to $r = 1$ mm, a value usually assumed for raindrops (e.g. Zsom et al. 2012). Fig. 4 shows the vertical cloud density distribution for different surface temperatures. Independent of the set-up the cloud remains at the same pressure between $10^{-3}-10^{-2}$ bar. For low surface temperatures, $T_{\rm surf} \lesssim 350$ K, the cloud is coupled to the surface and grows as the surface pressure increases. For higher surface temperatures the cloud density remains approximately constant. Around $T_{\rm surf} = 645$ K a second thin cloud layer emerges at the surface, as the rainout becomes very inefficient for such high pressures. However, due to its location deep in the optically thick region of the atmosphere the impact of the second cloud on the radiative transfer is minimal. Further, the second cloud disappears again for higher surface temperatures, as the BOA conditions exceed the critical point of water preventing any condensation. Also, the primary cloud begins to shrink for $T_{\rm surf} \approx 2000$ K as the dry adiabat penetrates the bottom of the cloud region removing condensates (compare Fig. 1 and Fig. 4).

2.5. *Condensate Size Distribution*

For the condensates we explore two different size distributions. Our fiducial model employs a log-normal distribution with the probability density function (pdf) p defined as

$$p(r) = \frac{1}{r\sqrt{2\pi}\ln\sigma}\exp\left[-\frac{1}{2}\left(\frac{\ln(r/\bar{r})}{\ln\sigma}\right)^2\right], \tag{8}$$

where r is the particle size, σ is the shape factor and $\bar{r}$ is the median radius.[5] We choose $\bar{r} = 10$ μm and $\sigma = 2$

[4] This value is estimated after the empirical data of Gunn & Kinzer (1949).

[5] The naming convention is unfortunately somewhat confusing. Often σ is referred to as the geometric standard deviation and $\tilde{\sigma} =$

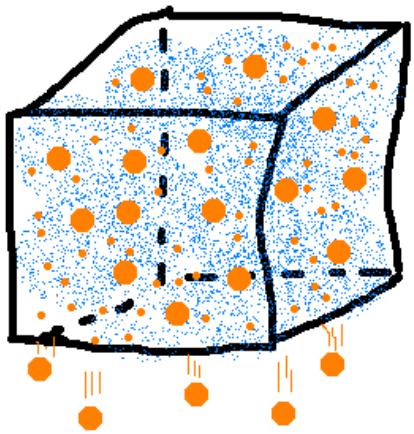

Figure 3. Atmospheric box toy model to estimate the amount of cloud condensates (small orange dots). Condensates aggregate and grow to water drops (large orange dots), which eventually rain out. In equilibrium the condensation rate equals the rainout rate.

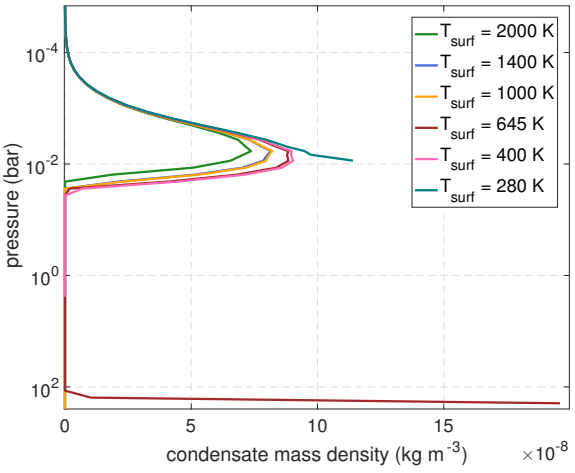

Figure 4. Vertical condensate (cloud) density distribution for different surface temperatures with the bulk located slightly above 10^{-2} bar independent of the set-up. Around $T_{\rm surf} = 645$ K a second cloud layer emerges but disappears for higher temperatures, which exceed the critical point of water.

following Zsom et al. (2012) and Ackerman & Marley (2001).

Secondly, we also explore a bimodal distribution, which is a convolution of two equally weighted gamma distributions i and j, with the pdfs given by

$$p_{i,j}(r) = \frac{r^{\alpha_{i,j}-1} e^{-r/\beta}}{\beta^{\alpha_{i,j}} \Gamma(\alpha_{i,j})}, \tag{9}$$

where $\alpha_{i,j}$ and β are the shape and scale parameters and Γ is the gamma function. In our case, the parameters are chosen $\alpha_{i,j} = 2.5$, 7.5 and $\beta = 4$ μm to describe two particle populations with median radii of 10 μm and 30 μm. The aim of this bimodal configuration is to represent a mixed population of liquid water droplets and ice crystals within the cloud. For simplicity we do not employ the latter distribution in our nominal model. However, we use it to test the impact of different particle size distributions on the cloud forcing (see Sect. 3.3).

In Fig. 5 the two described particle size distributions are displayed.

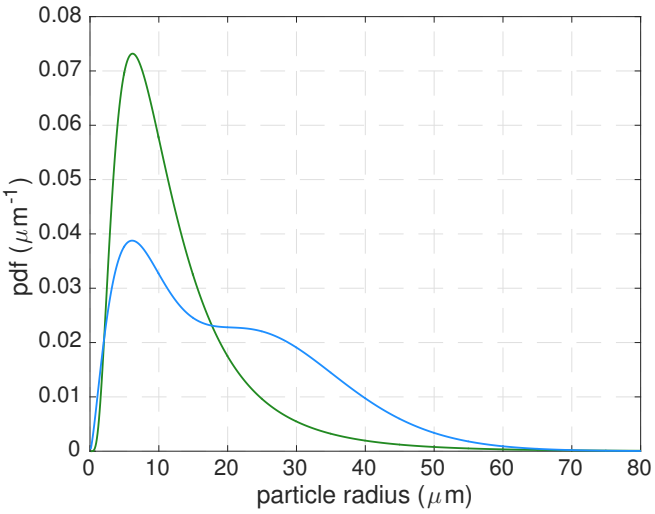

Figure 5. The pdfs of two particle size distributions explored in this study. The log-normal distribution (green) has a median radius of 10 μm and a shape factor 2. The bimodal gamma distribution (blue) is a convolution of two equally weighted gamma distributions with the shape parameters 2.5 & 7.5 and the scale factor 4 μm. The latter distribution describes a mixed particle population with pure water droplets and ice crystals with median radii of 10 μm and 30 μm, respectively.

2.6. *Cloud Optical Depth*

The general formula for the optical depth contribution of particles with radius r distributed over the width Δz is given by

$$\Delta\tau_{\rm cloud}(r) = Q_{\rm ext} \pi r^2 N(r) \Delta z, \tag{10}$$

where $N(r)$ is the number density of the cloud particles and $Q_{\rm ext}$ is the extinction efficiency parameter. The latter modifies the cross-sectional area πr^2 to obtain the effective value relevant for absorption and scattering of radiation of a certain wavelength. In our case we take Δz to be the width of an atmospheric layer and use a

$\ln\sigma$ the standard deviation. The median $\bar{r}$ is not to be confused with the mode of the radius $r_{\rm mode} = \bar{r}\exp\left[-(\ln\sigma)^2\right]$, which is the radius of highest probability, or the mean radius $r_{\rm mean} = \bar{r}\exp\left[(\ln\sigma)^2/2\right]$.

Mie-scattering code to calculate $Q_{\rm ext}$ for a given particle size distribution. The total optical depth for cloud particles of different sizes is then obtained by

$$\Delta\tau_{\rm cloud,tot} = \int_0^\infty \frac{d\tau_{\rm cloud}(r)}{dr}\, dr, \tag{11}$$

where we integrate over all occurring particle sizes. The dependence of the number density on the particle radius is given by

$$\frac{dN(r)}{dr} = p(r)N_{\rm tot} = p(r)\frac{\rho_{\rm cloud}}{\bar{m}_{\rm cond}}, \tag{12}$$

where $p(r)$ is the pdf of the particle size distribution used and $N_{\rm tot}$ the total number density of condensates of all sizes. We express the latter with the cloud mass density (eq. 7) and the mean condensate mass

$$\bar{m}_{\rm cond} = \int_0^\infty \frac{4}{3}\pi r^3 p(r)\, dr. \tag{13}$$

Figure 6 shows the cloud optical depth per atmospheric layer relative to pressure and wavelength for $T_{\rm surf} = 645$ K. Consistent with the cloud location, described in Sect. (2.4), the cloud impacts mainly the region around 10^{-2} bar. Also visible is the thin surface cloud, located deep in the optically thick region of the atmosphere. The wavelength dependence is a direct consequence of a varying $Q_{\rm ext}$ with wavelength. We show the nominal case of a log-normal particle size distribution centered around 10 μm, where the wavelength dependency is somewhat modest and peaks around $\lambda = 2\pi r$, which is here in the mid-infrared around 60 μm. Adding the individual layer contributions, the total optical depth of the main cloud at 10^{-2} bar is around $\tau_{\rm cloud} \sim 0.15 - 0.2$ depending on the wavelength.

Since the forcing of a cloud with such a small optical depth is limited, we mainly investigate cases with $10\times$ and $100 \times \tau_{\rm cloud}$, leaving the shape of the cloud intact. By this we combine the physical method of using the convective latent heat release to determine the location and shape of the cloud with a flexible parameter set for the final cloud forcing.

3. RESULTS

In this section we describe the results obtained by including our cloud model into the Earth's atmosphere clear-sky set-up (see Sect. 2.2 & 2.2.1), following in the footsteps of Goldblatt et al. (2013), and explore the effect of the clouds on the energy budget of the atmosphere.

3.1. *Greenhouse for Extended Temperatures*

Similar to the results found by Goldblatt et al. (2013), described in Sect. 1.1, we find the the clear-sky limits of 284 W m^{-2} for the net TOA shortwave flux and the maximum of 282 W m^{-2} for the outgoing TOA longwave

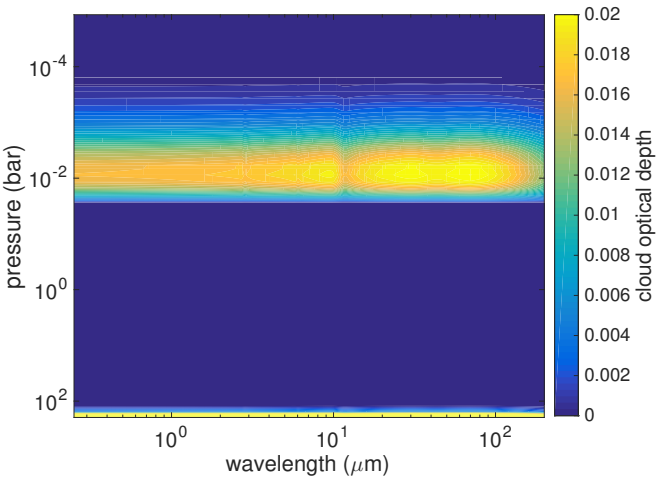

Figure 6. The cloud optical depth per atmospheric layer relative to pressure and wavelength for $T_{\rm surf} = 645$ K. The condensates follow here a log-normal size distribution centered at 10 μm. The cloud optical depth shows a modest wavelength dependency peaking in the mid-infrared around 60 μm, consistent with the condensate size. Adding the individual layer contributions, the total optical depth of the main cloud at 10^{-2} bar is around $\tau_{\rm cloud} \sim 0.15 - 0.2$ depending on the wavelength.

flux.[6] The resulting net flux of 2 W m^{-2} causes the atmosphere to steadily warm and induces a runaway. Fig. 7 shows the clear-sky behaviour of the atmosphere in blue color.

Introduction of the clouds has two main effects. First, the clouds increase the albedo by reflecting more incoming shortwave radiation and thus cooling the atmosphere (see Fig. 7, left panel). For the clouds with $\tau_{\rm cloud} = 1.7$ this reduction leads to a net shortwave flux change of -38 W m^{-2} at TOA once the clouds fully establish at $T_{\rm surf} \gtrsim 350$ K. Second, the clouds increase the optical thickness of the atmosphere towards planetary thermal emission (see Fig. 7, middle panel). In this particular cloud case, as the photosphere is moved to atmospheric layers with lesser temperatures and less emission, the outgoing longwave flux is decreased about 30 W m^{-2} compared to the clear-sky case. For a given shortwave absorption the decrease of thermal emission effect would usually lead to higher atmospheric temperatures. Here, the total cloud forcing, defined as the sum of the net shortwave net longwave forcings, leads to -8 W m^{-2} (see Fig. 7, right panel). A negative number means that the reduction in the shortwave absorption dominates and thus the net cloud forcing represents a net

[6] As expected, the limiting flux values differ marginally from the ones in Goldblatt et al. (2013), because we use updated H_2O absorption coefficients and a slightly altered numerical scheme compared to the previous study.

cooling. In fact, the clouds have a stabilizing effect by altering the atmospheric energy budget in a way that allows a stable equilibrium point around $T_{\rm surf} = 420$ K.[7] Increasing the cloud optical depth to $\tau_{\rm cloud} = 17$ magnifies the described mechanism.

3.2. *Cloud Forcing in Detail*

In this section we focus on one specific atmospheric set-up with $T_{\rm surf} = 645$ K. In addition, to the cloud cases presented before, we explore here cloud optical depths $\tau_{\rm cloud} = 0.1 - 170$ and instead of only switching the clouds on or off, we also vary the global cloud coverage fraction between 0 (no clouds) and 1 (full coverage). The effects for the shortwave flux are shown in the top panel of Fig. 8, for the longwave flux in the middle panel and the net flux in the bottom panel. As expected, the cloud forcing increases in general with cloud optical depth as well as coverage.[8] A vanishing net flux represents the boundary between stable and unstable atmospheres. Hence above a certain threshold thickness, clouds prevent a greenhouse runaway by causing the TOA net flux to be negative. This threshold is around $\tau_{\rm cloud} = 0.6$ for total cloud coverage and increases with less cloud coverage. Independent of cloud thickness there is no stable solution below a coverage fraction of 0.02. The impact of $\tau_{\rm cloud} = 1.7$ thick clouds with 50% cloud cover on the net flux for different surface temperatures is shown in Fig. 7, right panel.

In the following we focus on the attenuation and emission of the shortwave and longwave fluxes in the two nominal cases where the clouds have optical depths of $\tau_{\rm cloud} = 1.7$ and 17, shown in Fig. 9 by dashed and dot-dashed lines, respectively. Remember from Sect. 2.4 that the primary cloud location is around $P = 10^{-3} - 10^{-2}$ bar with a second thin cloud layer at the surface.

In the cloud-free case (solid line) the shortwave direct downward radiation is gradually attenuated by water absorption and scattering (Fig. 9, left panel). As water is a rather poor absorber in the optical a large fraction of the solar radiation reaches the deeper atmospheric layers where $P \gtrsim 10^{-1}$ bar. Through the Rayleigh mechanism water molecules scatter a fraction of the stellar rays back- and forward, forming the diffuse shortwave radiation. This happens around $P \sim 1$ bar as the atmosphere needs to be sufficiently thick for the Rayleigh scattering to have a significant impact. The clouds shift the main extinction of shortwave flux upward to the cloud layer as the clouds themselves already possess an optical depth $\tau_{\rm cloud} > 1$ dominating the molecular influence. The thicker the cloud the higher up the optical depth of unity is reached. Hence, thicker clouds absorb and scatter the shortwave radiation at higher levels.

The longwave radiation is very small in the top layers and slowly grows as more and more shortwave radiation is absorbed and re-emitted thermally with increasing atmospheric optical depth. Since thermal emission is isotropic the magnitude of the downward and upward longwave fluxes converges for deeper and optically thick layers. When inserting the clouds, the upward longwave radiation decreases as the main emission originates from higher and thus cooler atmospheric layers with increasing cloud thickness. Below the cloud layers the upward thermal emission is very similar to the clear-sky case. The downward longwave flux is somewhat enhanced with the insertion of clouds as the additional cloud optical depth also necessarily leads to an increase in thermal emission.

Fig. 9, right panel, shows the resulting net shortwave and longwave fluxes. The TOA values correspond to the ones visible in Fig. 7. By absorbing and reflecting incoming shortwave radiation on the one hand and damping longwave outward emission on the other hand, clouds attenuate both the short- and longwave net fluxes in the atmosphere. With thicker clouds the resulting net flux shifts to smaller values and as discussed above a certain thickness to negative values, effectively avoiding the runaway regime.

3.3. *Impact of the Size Distribution*

For the exploration of the effect of using a bimodal gamma distribution for the particle sizes, as described in Sect. 2.5, we employ the same atmospheric set-up as in the last section with $T_{\rm surf} = 645$ K. Fig. 10 shows a comparison between a model with the lognormal condensate size distribution (solid) and the bimodal distribution (dashed). We find that for clouds with $\tau_{\rm cloud} \lesssim 1.7$ the effect of the size distribution is insignificant. Hence, in Fig. 10 we show the thick cloud case with $\tau_{\rm cloud} = 17$ to make the effect visible. The main difference between the two test cases lies in the strength of the forward and backward scattering of the solar radiation. As the average particle size is larger in the bimodal case compared to the lognormal case, the forward scattering is somewhat enhanced and the backscattering diminished (see Fig. 10, left panel). This results in a 12 W m^{-2} higher value for the TOA net flux in this particular set-up.

[7] Equilibrium means here that the same amount of energy escapes the atmosphere as it enters. Stable means that a slight deviation in surface temperature alters the atmospheric interplay of transmission, absorption and scattering in such a way that the surface temperature is pushed back to the equilibrium value.

[8] This monotonic behaviour is broken for very thin clouds with $\tau_{\rm cloud} \lesssim 0.2$. This subtlety is a result of the wavelength dependent extinction efficiency of the cloud condensates.

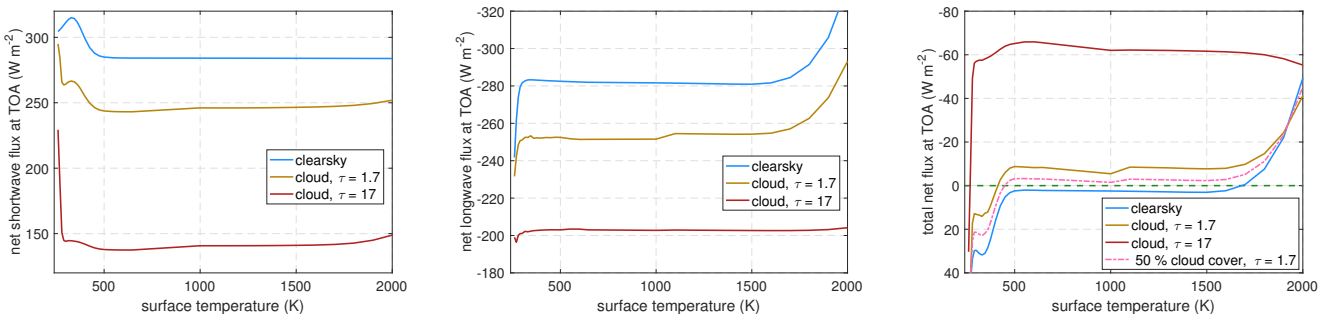

Figure 7. Comparison of a clear-sky model (blue) and two cloud models with $\tau_{\rm cloud} = 1.7$ (yellow) and $\tau_{\rm cloud} = 17$ (red) for different surface temperatures. The clear-sky limits for the net TOA shortwave flux and the outgoing TOA longwave flux are 284 W m^{-2} and 282 W m^{-2}, respectively, leading to a runaway greenhouse effect, due to a net incoming flux of 2 W m^{-2}. Clouds with $\tau_{\rm cloud} = 1.7$ cause a net cooling in the atmosphere leading to a net TOA flux of -6 W m^{-2} and have thus a stabilizing effect such that a runaway cannot establish. Setting $\tau_{\rm cloud} = 17$ enhances the cooling further. Also shown in the right panel as dashed line, is the nominal case with $\tau_{\rm cloud} = 1.7$ but only at a cover fraction of 50%. Also in this case the net cooling is enough to shift the net flux to negative values and lead to a stable atmosphere.

4. DISCUSSION & CONCLUSIONS

4.1. *Comparison to Previous Studies*

As the runaway greenhouse is a severe potential threat to the eco-system of a planet, numerous studies have explored upper bounds on the thermal outgoing flux of the Earth's atmosphere.

However, due to the complexity of cloud physics earlier studies focused on clear-sky conditions. For instance, Ishiwatari (2002) found that a thermal runaway occurs if the solar constant exceeds 1600 W m^{-2} using a 3D GCM (global circulation model) and a 1D radiative radiative-convective model. This would correspond to a spherically mean Simpson-Nakajima limit of 400 W m^{-2}. Their subsequent study Ishiwatari & Hayashi (2007) compares their GCM model with a 1D energy-balance model (EBM) by searching for possible equilibrium states for various solar constants and ice-cover fractions of the surface. They find a lower limit of 1310 W m^{-2} for the solar constant (327.5 W m^{-2} averaged irradiation), for which runaway may happen given an initially ice-free surface. Both values are significantly higher than what has been found by Goldblatt et al. (2013) and us.

More recent studies often have built-in clouds into their models; either in a simple 1D column format or more complex GCM.

The 1D approach was used e.g. by Goldblatt & Zahnle (2011). They explored the past Earth's climate in terms of the faint young sun paradox (FYSP). They implemented clouds at different altitudes and investigated their radiative effect (forcing) on the atmospheric energy budget. They found that the cloud forcing is strongly depending on the altitude of the clouds. Clouds high up in the atmosphere have a strong impact on both short- and longwave radiative transfer. If they are located in between the optical and thermal photosphere, the shortwave influence should dominate. Located below both photospheres the cloud impact should be negligible. This is consistent with our study. In our case the clouds are located above the shortwave photosphere (at $\sim 10^{-1}$ bar), but roughly coincide with the longwave photosphere (at $\sim 10^{-2}$ bar), and their effect on shortwave reflection appears to be larger than on the thermal emission. In general, they found a cloud forcing of less than 15 W m^{-2} for plausible set-ups. Our nominal cloud case leads to a cloud forcing of -8 W m^{-2} consistent with their range of plausible values.

The study of Leconte et al. (2013) also investigated the irradiation limit for the runaway greenhouse transition by combining a GCM with clouds. Their clouds are located so high in the atmosphere that their radiative forcing tends to vanish. However, due to their 3D grid, unsaturated atmospheric regions created by the Hadley circulation work as stabilizers and shift their value for the Simpson-Nakajima limit relatively high up to 375 W m^{-2}.

Finally, Wolf & Toon (2015) use a similar approach as Leconte et al. (2013), but set the clouds to deeper atmospheric layers. By this they have a stronger effect on the shortwave radiation and provide a negative feedback. They find the runaway to set in at 21% increased solar irradiation, corresponding to a value of 413 W m^{-2}. Earlier though, they encounter an additional stable atmospheric state called the moist greenhouse at 12.5 % increased irradiation or 384 W m^{-2}. This state is marked by a very high humidity and with increased surface temperature also evaporative water loss to space. They argue that for $T_{\rm surf} > 363$ K even though a stable moist atmosphere is possible the state is too short-lived and should also lead to water-poor atmospheres over longer time frames.

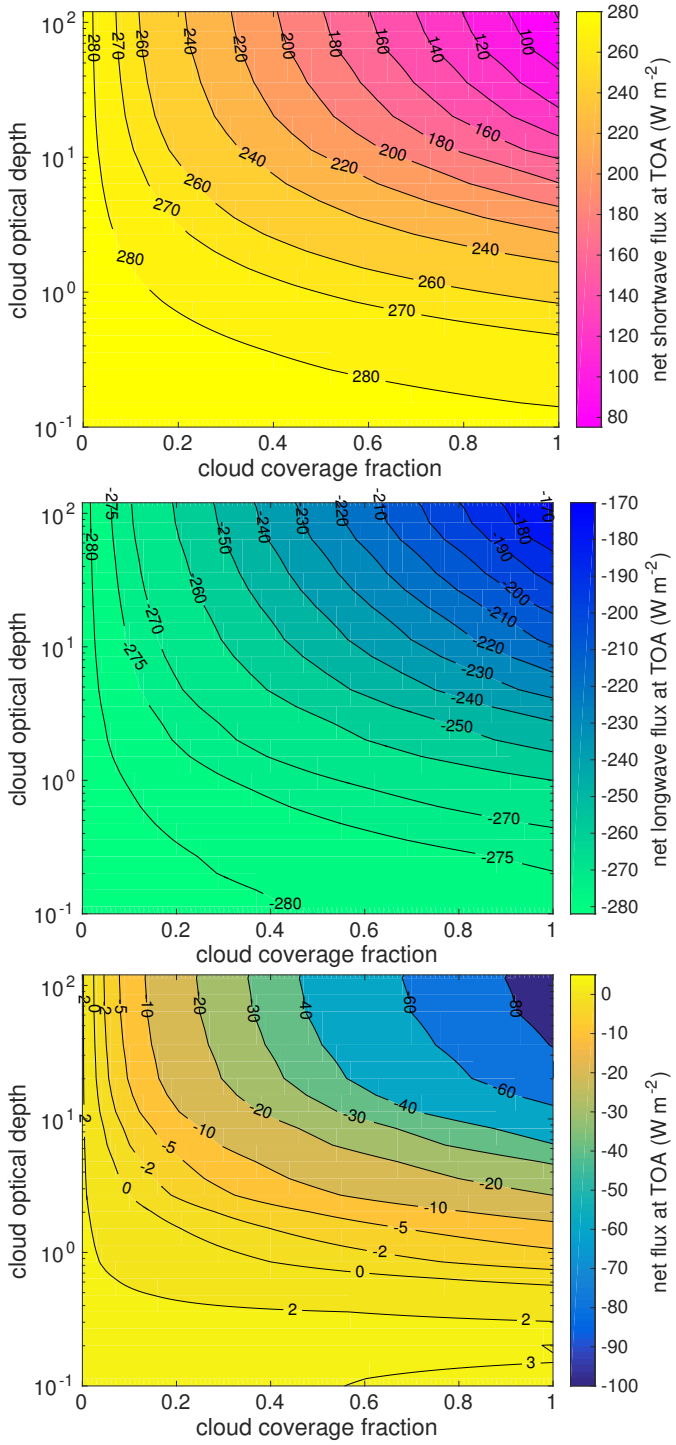

Figure 8. Net shortwave (top), net longwave (middle) and net flux (bottom) versus cloud optical depth and cloud cover fraction for $T_{\rm surf}$ = 645 K. In general, the cloud forcing increases with cloud optical depth as well as coverage. Thick clouds, where the TOA net flux is negative, allow for a stable equilibrium atmosphere and thus prevent a greenhouse runaway. The threshold for stability is around $\tau_{\rm cloud} = 0.6$ for total cloud coverage and increases with less cloud coverage. There is no stable solution below a coverage fraction of 0.02.

4.2. *Future Outlook*

Due to the strict time constraint given by the length of the Kavli Summer Program only the core tests could be conducted. In the following we present numerous possibilities to extend this study and make it more robust.

- In this work we have explored the atmospheric heating rates from the intergrated radiative fluxes. However, for observations signatures in the planetary spectral emission should be indicative as to whether a planet is in the runaway greenhouse regime. The brightness temperature (the temperature of the main emitting layer) being much lower than the effective temperature of the planet could be such a signature.

- As the simplest case we approximate the runaway in a pure water atmosphere. This is a good assumption for high temperatures where the water mixing ratio reaches unity due to liquid water evaporation independent of the initial atmospheric abundances at lower temperatures. However, the mixture of different molecules determines the relative strength of spectral bands and windows, which influences the ability to cool the atmosphere (c.f. Goldblatt et al. (2013) in the lower temperature range $T_{\rm surf} \sim 300$ K or in the higher end $T_{\rm surf} \sim 1600$ K). A more elaborate model could include other important greenhouse gases, e.g. CO_2, CH_4, CO, NH_3.

- Instead of assuming a fixed location for the primary cloud deck one can explore how the forcing changes with higher and lower altitude clouds. The radiative impact of clouds depends on their location relative to the atmospheric photosphere, e.g. below the photosphere the impact of clouds is expected to be inferior to the molecular extinction. The relative height of the clouds to the longwave and shortwave photospheres will determine the radiative impact of the clouds as discussed by e.g. Goldblatt & Zahnle (2011).

- In this study the cloud model is based on very simplified physical assumptions regarding condensation and rainout of cloud particles. The resulting cloud density is surprisingly low. A possible refinement would be the implementation of a convective scheme that mimics the updraft of cloud particles. This would partially counter the rainout rate and thus increase the cloud particle density.

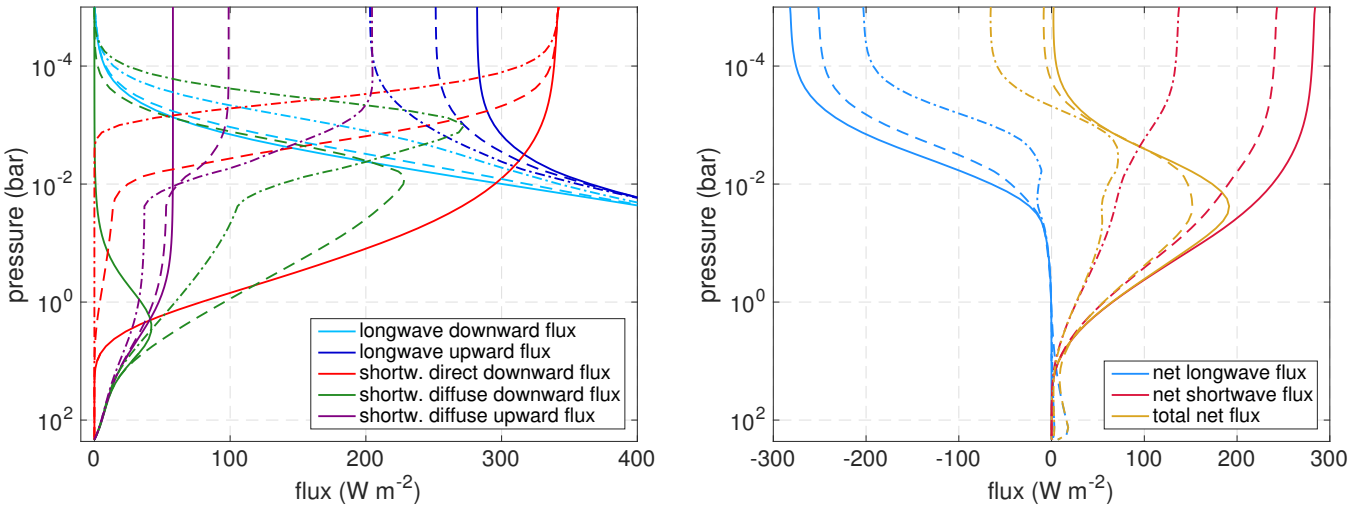

Figure 9. Comparison of a clear-sky model (solid) and two cloud models with $\tau_{\rm cloud} = 1.7$ (dashed) and $\tau_{\rm cloud} = 17$ (dot-dashed) for $T_{\rm surf} = 645$ K. The primary cloud is located around $P = 10^{-3} - 10^{-2}$ bar with a second thin cloud layer at the surface, see Fig. 4. With increasing optical thickness the clouds dominate the molecular extinction shifting the atmospheric photosphere upwards to the cloud location. Clouds significantly enhance scattering of shortwave radiation but simultaneously also dampen the planetary thermal emission, as the photosphere moves up to cooler temperatures. Sufficiently thick clouds lead in general to negative TOA net fluxes and have a stabilizing effect on the atmosphere.

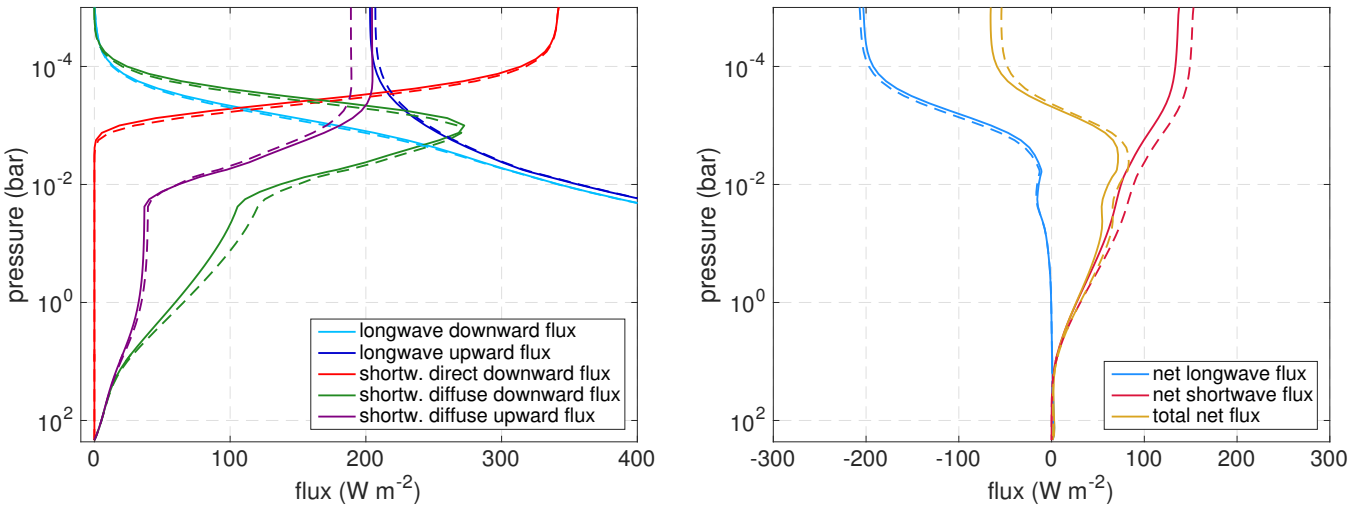

Figure 10. Comparison between a model with a log-normal condensate size distribution (solid) and a bimodal gamma distribution (dashed), see Sec. 2.5 for details. Here, $T_{\rm surf} = 645$ K and $\tau_{\rm cloud} = 17$. In the bimodal case the forward scattering is enhanced and the backscattering diminished compared to the log-normal case, which results in a 12 W m^{-2} higher value for the TOA net flux in this particular set-up.

ACKNOWLEDGEMENTS

The authors thank Tyler D. Robinson for sustained support when navigating the SMART and Mie-scattering codes employed in this study. They further thank the SOC and LOC of the 2016 Kavli Summer Program fur such an intellectually stimulating environment, and the Kavli Foundation for their gracious financial support.

REFERENCES

Ackerman, A. S., & Marley, M. S. 2001, ApJ, 556, 872
Goldblatt, C., Robinson, T. D., Zahnle, K. J., & Crisp, D. 2013, Nature Geoscience, 6, 661
Goldblatt, C., & Watson, A. J. 2012, Philosophical Transactions of the Royal Society of London Series A, 370, 4197
Goldblatt, C., & Zahnle, K. J. 2011, Nature, 474, E1
Gunn, K. L. S., & Kinzer, G. D. 1949, Meteorology, 6, 243 251
Ingersoll, A. P. 1969, Journal of Atmospheric Sciences, 26, 1191
Ishiwatari, M., K. N. S. T., & Hayashi, Y.-Y. 2007, J. Geophys. Res. Atmos., 112, doi:10.1029/2006JD007368
Ishiwatari, M., T. S. N. K. . H. Y. Y. A. 2002, J. Atmos. Sci., 59, 32233238
Komabayashi, M. 1967, J. Meteorol. Soc. Jpn., 45, 137
Leconte, J., Forget, F., Charnay, B., Wordsworth, R., & Pottier, A. 2013, Nature, 504, 268
Meadows, V. S., & Crisp, D. 1996, J. Geophys. Res., 101, 4595
Nakajima, S., Hayashi, Y.-Y., & Abe, Y. 1992, Journal of Atmospheric Sciences, 49, 2256
Simpson, G. C. 1927, Mem. R. Meteorol. Soc., 11, 69
Stamnes, K., Tsay, S.-C., Jayaweera, K., & Wiscombe, W. 1988, ApOpt, 27, 2502
Wolf, E. T., & Toon, O. B. 2015, J. Geophys. Res. Atmos., 120, doi:10.1002/2015JD023302
Zsom, A., Kaltenegger, L., & Goldblatt, C. 2012, Icarus, 221, 603